Insights into the Impact of Activators on the 'Catalytic' Graphitization to Design Anode Materials for Lithium Ion Batteries

Vanessa Hanhart+,[a] Lars Frankenstein+,[a] Joaquin Ramirez-Rico,[b] Vassilios Siozios,[a] Martin Winter,[a, c] Aurora Gomez-Martin,*[a] and Tobias Placke*[a]

In this work, we systematically investigate the 'catalytic' graphitization of a biomass precursor (coffee ground) using 10–60 wt.% of the activator iron (III) chloride hexahydrate in a temperature range of 1000 °C – 2400 °C. Special focus is put on the correlation of synthesis conditions, e.g., heat treatment temperature and mass fraction of iron chloride, with the electrochemical performance in carbon∣∣Li metal cells. The structural investigations of the materials reveal a positive impact of an increasing heat treatment temperature and/or mass fraction of inserted activator on the degree of graphitization and the delithiation capacity. However, a saturation point regarding the maximum degree of graphitization at 2000 °C and reversible capacity by the 'catalytic' graphitization approach using iron (III) chloride has been found. A maximum degree of graphitization of $\approx$69 % could be reached by applying 2000 °C and 40 wt.% $FeCl_3 \cdot 6H_2O$, resulting in a reversible capacity of 235 mAh g^{-1}.

Introduction

While the first generation of commercial lithium ion batteries (LIBs) was based on $LiCoO_2$ and soft carbon as active materials for positive (cathode) and negative electrode (anode), the third generation of LIBs, which entered the market in 1993–1994, was based on $LiCoO_2$∣∣graphite. Now, almost 30 years later, graphite is still the state-of-the-art active material for the anode of LIBs.[1] Graphite exhibits a theoretical capacity of 372 mAh g^{-1} (on the basis of the mass of the graphite host) when fully lithiated to LiC_6 in combination with a flat potential plateau and low average (de)lithiation potential ($\approx$0.2 V vs. Li∣Li$^+$) as well as a low voltage hysteresis, thus, a high voltage and energy efficiency.[2] In contrast to emerging Si/C composites, which

feature a significantly higher specific capacity depending on the Si content (theoretical specific capacity of 3579 mAh g^{-1}),[3] graphite expands only slightly during lithiation (up to $\approx$10 %), leading to a highly effective solid electrolyte interphase (SEI[4]) formation in suitable electrolytes, which in turn enables an outstanding long-term cycling stability.[5] It is foreseeable that the LIB technology will dominate the rechargeable battery market for at least the next decade, and graphite will continue to play a major role as anode material.[2b,6]

Two types of graphite are available on the market for the application in LIBs, i.e., natural graphite (NG) and synthetic/artificial graphite (SG).[2b,6a] There is an ongoing debate about which form of graphite is the most appropriate to be used as anode material. Currently, there is a growing trend to use mixtures of NG and SG to maximize cost savings, power, capacity, and lifetime benefits.[7] Even though SG-based anodes dominate the LIB market ($\approx$60 % in 2020) compared to NG ($\approx$40 % in 2020), this will shift to larger shares of NG due to supply limitations of SG.[7] Nevertheless, NG is considered as a 'critical' raw material by the European Union and the U.S.. The world's largest deposits are in China.[8] In addition, the supply of SG is determined by the availability of petroleum coke (so-called "needle coke"),[9] which in turn is significantly dominated by China.[7,10] There are various environmental and economic challenges in graphite supply chains.[11] For example, emissions are generated during graphite production or mining and subsequent processing, which can have negative impacts if not properly controlled through EHS (environment, health and safety) measures during processing. This includes high environmental impacts, such as air and water pollution from purification of NG using acids.[11]

NG is defined as a mineral found in nature,[12] which is formed under metaphoric conditions, i.e., high pressure and temperature. Therefore, it occurs in different shapes and levels

[a] V. Hanhart,+ L. Frankenstein,+ Dr. V. Siozios, Prof. Dr. M. Winter, Dr. A. Gomez-Martin, Dr. T. Placke
University of Münster
MEET Battery Research Center, Institute of Physical Chemistry
Corrensstr. 46, 48149 Münster, Germany
E-mail: agomezma@uni-muenster.de
          tobias.placke@uni-muenster.de

[b] Prof. Dr. J. Ramirez-Rico
Departamento Física de la Materia Condensada and Instituto de Ciencia de Materiales de Sevilla
Universidad de Sevilla – CSIC
Avenida Reina Mercedes SN, 41012 Sevilla, Spain

[c] Prof. Dr. M. Winter
Helmholtz Institute Münster
IEK-12, Forschungszentrum Jülich GmbH
Corrensstr. 46, 48149 Münster, Germany

[+] These authors contributed equally to this work.

of purity. For the application in LIBs, a consistently high quality in terms of purity and morphology is required, which can only be achieved through a series of refinement and purification steps. Thermal and chemical treatments, *e.g.*, acid treatments (*e.g.*, HCl, HF or H_2SO_4) are used to produce highly pure graphite.[13] In contrast to NG, SG has no geographical restrictions regarding production. SG is synthesized by high temperature graphitization of graphitizable carbons,[6a,13a] resulting in a long-range ordered crystal structure. The main precursor is petroleum or "needle" coke,[9] a by-product of oil refinery.[14] Consequently, the final product cannot be considered as sustainable, as oil reserves are limited. Furthermore, high temperatures of $> 2800\,°C$ have to be applied during graphitization, which is cost and energy intensive.[6a,15]

Promising alternative precursors to produce carbon and SG anode active materials are (i) industrial waste or by-products and (ii) biomass, which is available in large scales (ideally in tons) and can be obtained with highly reproducible material characteristics. There is a great effort in literature to make biomass available as precursor materials for the synthesis of not only highly ordered graphite, but also activated carbons and hard carbons.[16] Heat treated biomass typically forms "non-graphitizable" carbons, which possess a randomly oriented nanotexture including cross-linked crystalline and amorphous regions. Due to rigid cross-linking of the individual carbon domains, a long-range order of the crystal lattice cannot be reached for non-graphitizable carbons, even though high temperatures are applied.[17] The approach of 'catalytic' graphitization is applied typically on "non-graphitizable" carbons to enable a reorganization of the crystal lattice and, thus, a long-range order of the structure.[16b,18] In this process, a so called 'catalyst', which typically consists of transition metals (Fe, Co, Ni, *etc.*), is introduced either wet or dry into a precursor material (*e.g.*, by impregnation with a solution of $FeCl_3$).[16b,18c] Subsequently, carbonization and graphitization in form of a heat treatment is applied, followed by removal of the 'catalyst' by acid etching. However, the term 'catalyst' is in most cases not suitable since the substance is consumed during reaction. According to IUPAC, such substances should be called 'activators'.[19] Therefore, the term 'activator' will be used in this work. In previous works, iron showed the highest catalytic activity in non-graphitizing carbons often attributed to their d-electron configuration and free electron vacancies, which will enable the formation of strong covalent bonds between metal particles and carbon atoms.[18a,20]

Several previous works have reported the possible structural transformation from amorphous to graphitic carbon of biomass using Fe as additive.[16b,21] Unfortunately, there are almost no systematic studies concerning process parameters, *e.g.*, heat treatment temperature and concentration of activator, and their impact on not only material properties, *e.g.*, specific surface area, degree of graphitization and crystal size, but especially on the resulting electrochemical performance as anode materials in LIB cells. Gomez-Martin *et al.*[16b] showed an enhanced degree of graphitization of a hard wood-based precursor with increased heat treatment temperatures (850–2000 °C) when using iron chloride as activator at a fixed concentration and observed improved specific capacities of the produced carbons. Sagues *et al.* used iron powder to catalyze the conversion of softwood, hardwood, cellulose, glucose, and lignin precursors to crystalline graphite at 1200 °C.[22] A maximum reversible capacity of $\approx 344\,mAh\,g^{-1}$ was reported for the softwood-derived graphite in Li metal cells. More recently, Banek *et al.* reported the conversion of hardwood sawdust to highly crystalline graphite flakes by laser pyrolysis using iron powder with similar maximum reversible capacities as known for commercial synthetic graphites.[23]

In this work, high temperature graphitization of coffee grounds as biomass precursor with the activator iron (III) chloride hexahydrate ($FeCl_3 \cdot 6H_2O$) was investigated with special focus on the impact of heat treatment temperature and the concentration of the activator on structural properties and electrochemical performance in carbon||Li metal cells. Figure 1 illustrates the synthesis procedure, including (i) impregnation with the activator solution ($FeCl_3 \cdot 6H_2O$ in isopropanol), (ii) carbonization/graphitization, (iii) removal of the activator by acid washing and (iv) particle size control by sieving. Subsequently, the synthesized carbons are characterized by several structural and electrochemical methods. Heat treatment temperatures between 1000 °C and 2400 °C, and concentration of activator between 0 and 60 wt.% were investigated.

Results and discussion

Analysis of mass loss during initial carbonization

Coffee grounds are mainly composed of cellulose, hemicellulose, proteins and ashes, resulting in high proportions of heteroatoms, *e.g.*, nitrogen and oxygen.[24] These structures easily decompose into gaseous components at increased
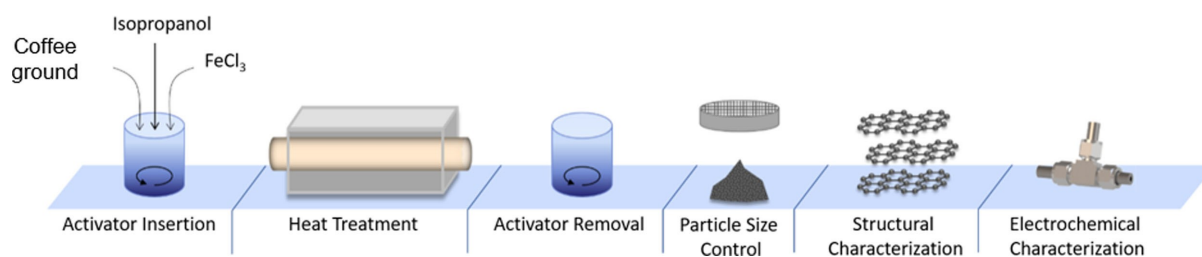

Figure 1. Overview of carbon material synthesis, processing and evaluation in this work.

ChemElectroChem

Research Article
doi.org/10.1002/celc.202200819

**Chemistry
Europe**

European Chemical
Societies Publishing

temperatures (*e.g.*, CO_2, CO, NO_x), leading to a significant weight loss and resulting in a carbonaceous sample. Thermogravimetric analysis was carried out to determine the exact mass loss during carbonization under argon atmosphere (Figure S1), whereby a total mass loss of ≈ 80 wt.% was determined up to a temperature of $1200\,°C$. The carbon yield from the coffee grounds carbonization can thus be estimated to be ≈ 20 wt.% based on dry biomass weight. The major mass loss (> 70 wt.%) occurs in the range from ≈ 200 to $500\,°C$.

Determination of mass fraction of iron present in carbonaceous samples after heat treatment

The real iron content in the samples was determined by inductively coupled plasma-optical emission spectrometry (ICP-OES), since the Fe/C-ratio changes during heat treatment due to mass loss. Therefore, samples containing 10, 20, 30, 40 and 60 wt.% $FeCl_3 \cdot 6H_2O$ (based on the mass of carbon obtained after the carbonization process of coffee grounds without activator) were carbonized at $1000\,°C$ and graphitized at $2000\,°C$ for 10 h under argon atmosphere. The resulting mass fractions of iron after the heat treatments can be seen in Table 1.

The mass fraction of iron present in carbonized samples at $1000\,°C$ increases linearly with the concentration of $FeCl_3 \cdot 6H_2O$ in the impregnation solution. However, after heat treatment at $2000\,°C$, there is almost no iron detectable due to dehydration and decomposition of $FeCl_3 \cdot 6H_2O$ at temperatures $> 100\,°C$ as well as the use of temperatures significantly above the melting point of iron.[25] It has already been reported that the volatility of the $FeCl_3$ precursor might drive continous evaporation from the carbon precursor. If this would be true, the graphitization process can be limited due to the continous loss of the activator when increasing the heat treatment temperature. Hoekstra *et al.* investigated the graphitization of cellulose with different iron salts and found a similar behavior for $FeCl_3$.[21d]

Structural characterization of carbonaceous materials

Raman spectroscopy is a non-destructive method for the structural characterization of highly ordered solid materials with a crystalline long-range order. Furthermore, it is highly sensitive to structural disorder and thus, a helpful tool to investigate the extent of graphitic structures in carbonaceous materials.[26] Carbons feature several Raman signals, originating from different lattice vibrations within the graphene layers (Figure S2–S7). A perfectly ordered graphitic lattice exhibits only one first-ordered band, the G band ('graphite') at $1580\,cm^{-1}$.[27] It can be assigned to the in-plane bond-stretching motion of sp^2-hybridized carbon bonds with E_{2g}-symmetry.[26] However, graphitic carbons and carbonaceous materials comprise structural disorders in the graphitic lattice, causing the appearance of four additional first-ordered D bands ('defect').[26] The most pronounced D band is the D1 mode at $\approx 1360\,cm^{-1}$, which originates from graphitic lattice vibrations with A_{1g}-symmetry, occurring in direct vicinity of structural disorders, *i.e.*, at the edges of graphene layers or in presence of heteroatoms within the structure.[28] The D2 mode can be seen as a shoulder of the G band at $\approx 1620\,cm^{-1}$, featuring the same lattice vibration as the G band. This mode only occurs at graphene layers on the surface, which are not directly sandwiched by two other graphene layers.[28a,29] Thus, the relative peak area of the D2 mode can be considered as an indicator for the volume to surface ratio of the graphitic crystals or the stacking order of the graphene layers in c-direction (L_c). Besides, there are two more peaks visible: the D3 mode at $\approx 1500\,cm^{-1}$, originating from amorphous fractions and the D4 mode at $\approx 1200\,cm^{-1}$, due to the sp^2-sp^3 bonds of C–C and C=C stretching vibrations of polyene-like structures.[28a] Additionally, the first overtone of the D1 mode (2D) appears at $\approx 2700\,cm^{-1}$, which is influenced by the stacking order in c-direction. In literature, the intensity ratio of the D1 and G bands (I_{D1}/I_G), based on the raw data, is often used as an indicator for the extent of graphitization. However, a more accurate statement can be made by integrated intensity ratios, as the D2, D3 and D4 modes can be excluded.[28a] Therefore, the observed Raman spectra were fitted according to Sadezky *et al.*[28a] Based on the I_{D1}/I_G-ratio, the crystallite size in a-direction (L_a) can be calculated by equation (1) proposed by Cançado *et al.*[30] Furthermore, the degree of graphitization α ($0 \le \alpha \le 1$) can be calculated by equation (2) considering the integrated intensity areas.[31]

$$L_a = 2.4 \cdot 10^{-10} \cdot \lambda^4 \left(\frac{I_{D1}}{I_G} \right)^{-1} \tag{1}$$

$$\alpha = \frac{I_G}{I_{D1} + I_G} \tag{2}$$

First, the impact of heat treatment temperature (T_H) on the degree of graphitization was considered. Hence, carbonaceous materials, synthesized with 10 wt.% $FeCl_3 \cdot 6H_2O$ at T_H of $1000\,°C$–$2000\,°C$ and 20 wt.% $FeCl_3 \cdot 6H_2O$ at T_H of $1000\,°C$–$2400\,°C$, were investigated by Raman spectroscopy (Figure 2). Moreover, the impact of the activator concentration on the degree of graphitization was investigated as well. Therefore, carbonaceous materials containing 10, 20, 30, 40 and 60 wt.% $FeCl_3 \cdot 6H_2O$ were synthesized at $2000\,°C$. Representative Raman

Table 1. Present mass fractions of iron after carbonization and graphitization of coffee grounds samples impregnated with 10, 20, 30, 40 and 60 wt.% $FeCl_3 \cdot 6H_2O$ in isopropanol, determined by ICP-OES.

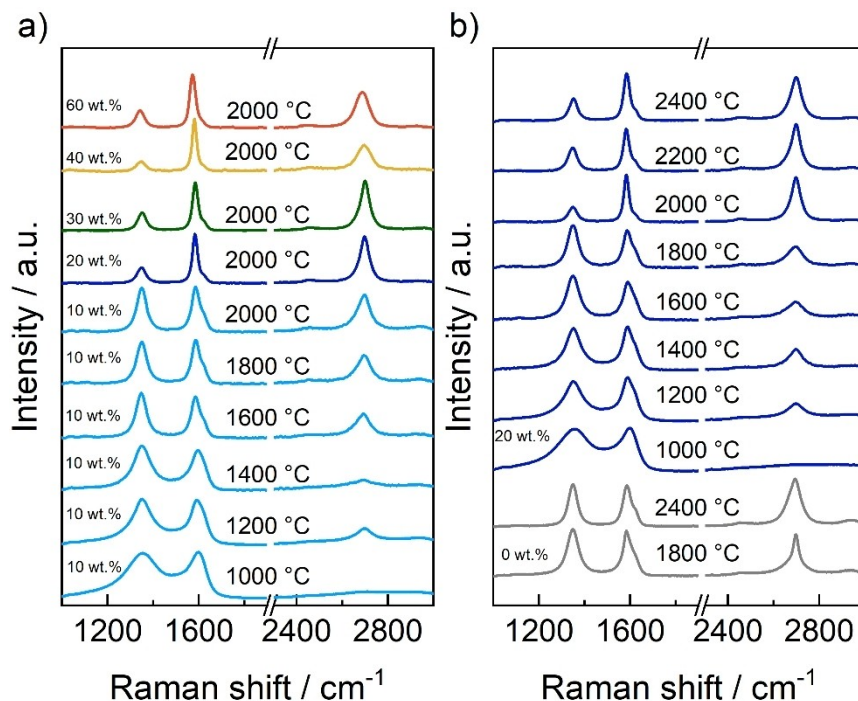| Inserted $FeCl_3 \cdot 6H_2O$/[wt.%]		Iron content/[wt.%]
10	after heat treatment at $1000\,°C$	4.48
20		7.88
30		11.90
40		14.88
60		17.88
10	after heat treatment at $2000\,°C$	0.01
20		0.01
30		0.09
40		0.02
60		0.07

Figure 2. (a, b) Raman spectra of carbonaceous materials synthesized with 0 wt.% (grey), 10 wt.% (light blue); 20 wt.% (dark blue), 30 wt.% (green), 40 wt.% (yellow) and 60 wt.% (red) $FeCl_3 \cdot 6H_2O$ at various T_H.

fits and detailed results can be seen in Figure S2–S7, Figure S8 and Table S1.

The Raman spectra of carbonaceous materials synthesized with 10 wt.% activator at $1000\,°C \geq T_H \leq 2000\,°C$ in 200 °C steps, exhibit the G band and all five D bands (Figure 2). The comparison of the respective spectra displays a pronounced D1 band throughout the whole temperature range, indicating a high proportion of structural disorder. The initial I_{D1}/I_G-ratio of 3.90 (± 0.7) at 1000 °C can be decreased to 1.5 (± 0.2) with an

increased T_H of 2000 °C (Figure S8c, Table S1). However, only a low degree of graphitization of 0.40 (± 0.03) can be reached (Figure 3) which is close to values reported in previous works without the use of iron.[32] The L_a value shows no significant changes throughout the whole temperature range, as it fluctuates between $\approx 5\,nm$ and 14 nm (Figure S8a). Moreover, the relative D2 peak area decreases from 5.8 % (± 0.2) to 4.2 % (± 0.3), indicating an ongoing stacking mechanism with increasing T_H (Figure S8b). However, in comparison to the activator-
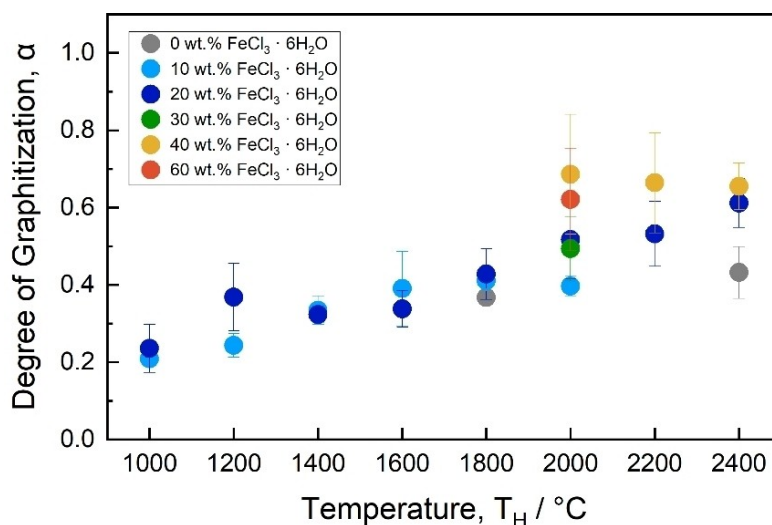

Figure 3. Degree of graphitization of carbonaceous materials synthesized with 0 wt.% (grey), 10 wt.% (light blue); 20 wt.% (dark blue), 30 wt.% (green), 40 wt.% (yellow) and 60 wt.% (red) $FeCl_3 \cdot 6H_2O$ at various temperatures (T_H). Error bars represent the standard deviation of at least 5 measurements per carbonaceous sample.

ChemElectroChem

Research Article
doi.org/10.1002/celc.202200819

**Chemistry
Europe**
European Chemical
Societies Publishing

free samples there is no significant improvement visible, leading to the assumption that 10 wt.% activator is not sufficient to reach high degrees of graphitization. In contrast, carbonaceous samples containing 20 wt.% activator during synthesis exhibit an almost linear decrease in the I_{D1}/I_G-ratio from 3.5 ($\pm$1.0) to 0.7 ($\pm$0.2) with increasing T_H (Figure S8c). Thus, the degree of graphitization (α) increases drastically from 0.24 ($\pm$0.06) to 0.61 ($\pm$0.06) with increasing T_H when using 20 wt.% activator. The crystallite size in a-direction increases slightly from $\approx$6 nm to 32 nm, as shown in Figure S8a. Moreover, the relative D2 peak area decreases from 5.9% ($\pm$0.4) to 2.7% ($\pm$0.5), indicating an increased stacking order with increasing T_H (Figure S8b).

Although an enhanced graphitization can be achieved by the application of higher heat treatment temperatures, an increased mass fraction of the activator might be beneficial for the development of a graphitic structure as well (Figure 2). Therefore, coffee ground, impregnated with different mass fractions of activator (10–60 wt.%), was graphitized at 2000 °C and the resulting carbonaceous materials were also structurally characterized by Raman spectroscopy. In this case, the degree of graphitization increases from 0.40 ($\pm$0.03) to 0.62 ($\pm$0.13), whereas the relative D2 peak area further decreases from 4.2% ($\pm$1.3) to 2.5% ($\pm$1.4) with increasing concentration of activator from 10 to 60 wt.%, while the L_a value increases almost linear from $\approx$13 nm to 40 nm, as shown in Figure S8 and Figure 3. The higher degrees of graphitization are achieved for the samples containing 40 or 60 wt.% activator at $T_H \geq 2000$ °C (Table S1). According to these results, there seems to be a

limitation using iron chloride for the graphitization of coffee ground as higher activator content or heat treatment temperatures have no further positive impact on the degree of graphitization.

The evolution of the graphitic structure can also be observed *via* powder x-ray diffraction (PXRD) analysis (Figure 4a, b and Figure S9). Graphitic carbon consists of perfectly stacked graphene layers with a minimal interlayer distance of 0.3354 nm, visible as a reflection at $2\theta \approx 26.6°$. However, most organic materials usually form non-graphitizing carbons, which are characterized by the evolution of a turbostratic phase, visible as a *002* carbon reflection at $\approx 26°$ in the XRD patterns.[33] The rotated graphene layers of turbostratic carbons lead to an increased interlayer distance of $\approx$0.344 nm. The interlayer distances of amorphous, turbostratic and graphitic fractions of carbonaceous materials can be determined by Bragg's law ($n\lambda = 2d \sin\theta$).[34] The 2θ-positioning of the carbon reflections was corrected previously by addition of 10 wt.% of sieved pure silicon powder as an internal standard (Figure S10). Here, the *002* reflections occurring in the range of 20–30° were fitted with three reflections (amorphous, turbostratic and graphitic) according to Iwashita et al.,[33] one for each structural appearance of carbon (Figure S9).

Figure S11 shows the evolution of the relative intensity of amorphous, turbostratic and graphitic carbon phases for all samples with regard to the heat treatment temperature. It can be observed that the amorphous phase seems to experience a continuous decrease with increasing treatment temperature, while the graphitic phase contributes up to 50% for the
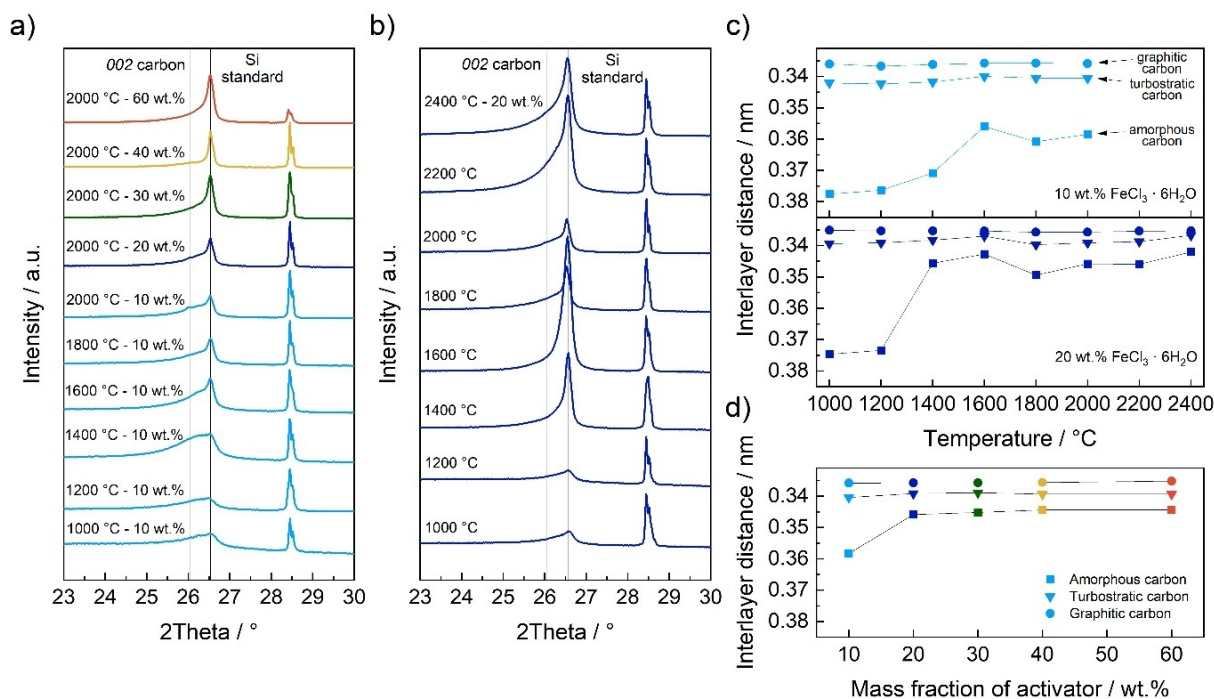

Figure 4. (a, b) XRD patterns and interlayer distances (c) at different temperatures and (d) at 2000 °C of coffee ground derived carbons containing 0 wt.% (black), 10 wt.% (light blue), 20 wt.% (dark blue), 30 wt.% (green), 40 wt.% (yellow) and 60 wt.% (red) FeCl$_3 \cdot$6H$_2$O during heat treatment. Vertical black lines point out the theoretical positions of the turbostratic and graphitic reflections of carbonaceous materials. Symbols with square, inverted triangle and circle shapes represent the contribution from amorphous, turbostratic and graphitic carbons, respectively.

ChemElectroChem

Research Article
doi.org/10.1002/celc.202200819

**Chemistry
Europe**
European Chemical
Societies Publishing

samples synthetized with 40 or 60 wt.% $FeCl_3$ at $T_H \geq 2000\,°C$. Increasing the activator content from 30 to 60 wt.% at a temperature of 2000 °C seems to have little beneficial effect on the degree of graphitization.

The resulting interlayer distances for each fraction can be seen in Figure 4c. The interlayer distance of the amorphous fraction decreases moderately in the case of samples synthe-sized with 10 wt.% $FeCl_3 \cdot 6H_2O$ until a plateau at ≈ 0.360 nm is reached (Figure 4c, top). In case of an activator content of 20 wt.%, a rapid decrease of the amorphous interlayer distance can be seen between 1200 °C and 1400 °C as a result of the increased degree graphitization promoted by using iron, resulting in an almost constant interlayer distance of ≈ 0.345 nm (Figure 4c, bottom). No significant differences were observed for the interlayer distance of graphitic and turbostratic reflections. At a graphitization temperature of 2000 °C (Fig-ure 4d), the sample containing 10 wt.% activator shows the larger interlayer distance for the amorphous contribution giving evidence of the high structural disorder, in agreement with Raman measurements. Higher concentrations of activator >10 wt.% result in a decreased interlayer distance for the amorphous contribution but it seems to remain almost constant from 20 wt.% activator content.

Analysis of particle and surface morphology of carbonaceous materials

The specific surface area of the carbonaceous materials was investigated by nitrogen adsorption measurements at 77 K. Resu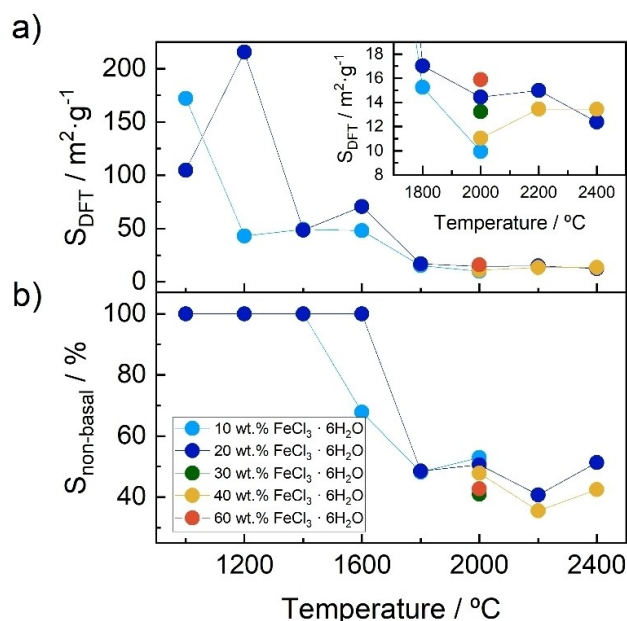lts are shown in Figure 5a, b. The resulting adsorption isotherms were evaluated by the BET theory to determine the specific BET surface area, whereas surface characteristics, *i.e.*, 'basal plane', and 'non-basal plane' (including 'prismatic' and 'defect') surface areas in graphitic samples, were calculated by DFT analysis based on the respective adsorption potentials (Table S1).[35]

The resulting physisorption isotherms were evaluated as type IV isotherms with an H3 hysteresis loop according to recommendations by IUPAC, *e.g.*, as shown in Figure S12 for carbons obtained at 2000 °C (20 wt.% $FeCl_3$).[36] Type IV isotherms exhibit an inflection point at low relative pressures, which is clearly visible in the isotherms of low temperature carbons, however, the inflection point levels off with increasing heat treatment temperature. The H3 hysteresis can be observed for adsorbents consisting of plate-like particles with slit-shaped pores,[36] which is also visible in the SEM images (Figure 6). The DFT surface area decreases throughout the whole temperature range for 10 and 20 wt.% activator content, stagnating at a surface area of ≈ 13 m^2 g^{-1}. The removal of activator particles by acid etching creates mesopores in the material, which can increase in size due to the formation of larger iron particles with increasing T_H.[16b] However, this effect seems to be outweighed by the total reduction of surface area due to a high mass loss during carbonization and the ongoing graphitization of the material, which leads to a denser structure.

Furthermore, all samples were investigated *via* SEM before sieving to investigate surface and particle morphology (Fig-ure 6). All samples consist of angular partly plate-shaped particles, containing slit-shaped macropores. There are no significant differences in morphology visible regarding different synthesis conditions, *i.e.*, heat treatment temperature and activator content, since the macroscopic shape of the precursor coffee ground is retained to a large extent.[37]

Electrochemical characterization of carbonaceous materials

The impact of synthesis conditions, *i.e.*, heat treatment temper-ature and iron chloride content, on the electrochemical performance in LIBs was investigated by constant current cycling (CCC) experiments of carbon‖Li metal cells using a three-electrode cell configuration with lithium metal as CE and RE (half-cell setup, control of WE potential).[38] CCC experiments were conducted using C-rates between 0.1 C and 10 C (1 C equals a specific current of 372 mA g^{-1}), and the resulting specific delithiation capacities can be seen in Figure 7. Figure 7a illustrates the performance of cells using the carbon samples synthetized at 2000 °C for 10–60 wt.% activator, while Figure 7b depicts the rate performance for cells with the samples obtained at either 2000 °C or 2400 °C for 20 or 40 wt.% activator.

From previous works, it is known that a higher degree of graphitization does not only lead to a higher specific capacity at lower rates, but can also limit the rate capability of the material.[16a,b] A major reason is the slower lithiation kinetics of the intercalation mechanism into graphitic layered structures compared to more amorphous structures where the lithium ion
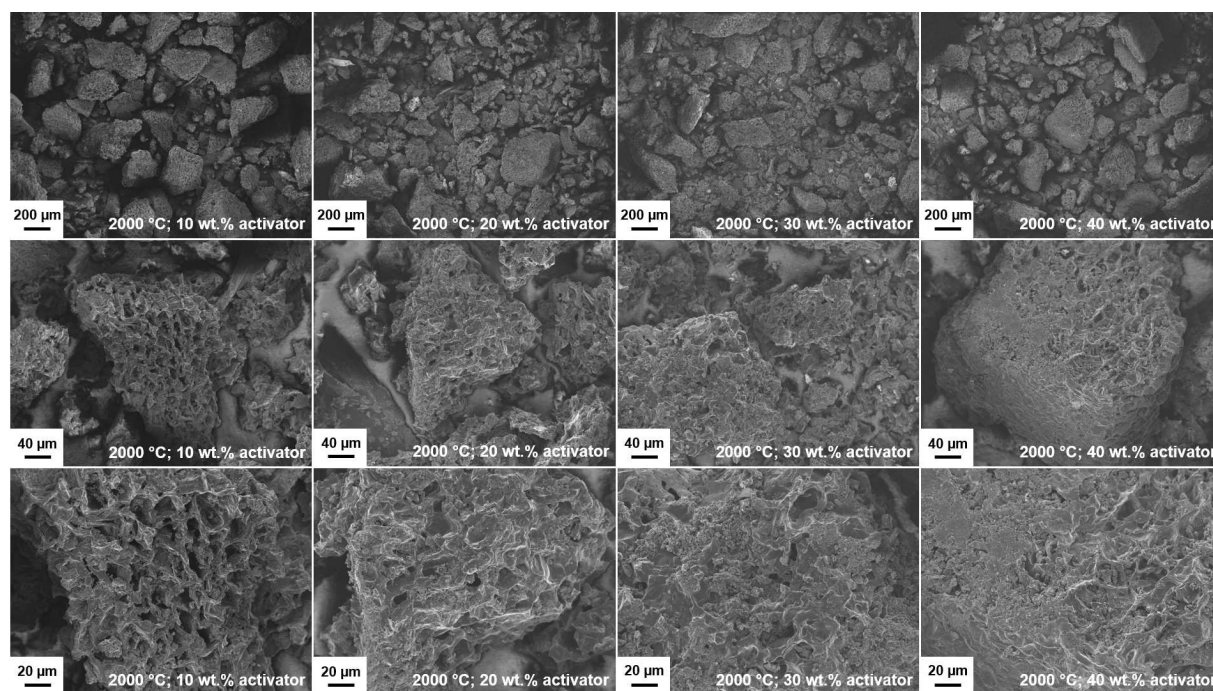

Figure 5. (a) DFT and (b) 'non-basal plane' surface area of coffee ground-derived carbons containing activator contents of 10 wt. - 60 wt.% during heat treatments in the temperature range of 1000 °C–2400 °C. 10 wt.% (light blue), 20 wt.% (dark blue), 30 wt.% (green), 40 wt.% (yellow) and 60 wt.% (red) $FeCl_3 \cdot 6H_2O$.

ChemElectroChem

Research Article
doi.org/10.1002/celc.202200819

**Chemistry
Europe**

European Chemical
Societies Publishing

Figure 6. SEM images of coffee ground-derived carbons containing 10–40 wt.% $FeCl_3 \cdot 6H_2O$ during heat treatment at 2000 °C.

storage mechanism mainly takes place by adsorption/insertion of Li^+ ions onto disordered graphene sheets, which is particularly noticeable to be benefited at high charge rates.[39] Furthermore, the SEI is formed within the first charging cycles due to electrolyte decomposition, which preferably passivates the prismatic graphite surfaces,[35b] thus, protecting against further electrolyte degradation and solvent co-intercalation. Li^+ ions must therefore first strip off their solvation shell to be able to pass the SEI, which is another reason for the poor rate capability of graphitic structures.[39a] This phenomenon is visible in the C-rate performance of samples containing a high mass fraction of iron during synthesis (Figure 7a), due to a more graphitic structure. While the carbonaceous samples synthetized at 2000 °C using 40 wt.% and 60 wt.% activator content deliver the highest capacity at 0.1 C, the capacity drop with increasing rates becomes more significant than for the other samples.

Moreover, an increased heat treatment temperature above 2000 °C seems to have little significant beneficial impact on the maximum specific delithiation capacity, especially for the high activator content (40 wt.%) samples (Figure 7b). The differential capacity (dQ/dV) plots and potential profiles of the different carbon materials are illustrated for the 1st and 4th cycles during de-/lithiation in Figure S13 and S14. In the 1st cycle lithiation curves, the potential plateaus (Figure S13c and S14c) and dQ/dV peaks (Figure S13a and S14a) between 0.9–0.8 V *vs.* Li|Li^+ correspond to electrolyte decomposition and SEI formation. In addition, it can be observed that the lithiation for all samples already starts at ≈ 0.8–1.0 V *vs.* Li|Li^+ (Figure S13d and S14d), which is an indication for lithium insertion into amorphous carbon. The highly graphitized samples, *e.g.*, the carbons

obtained at 2000 °C using 40 wt.% activator as well as the samples produced at 2400 °C using 40 wt.% activator, feature the characteristic peaks of the staging phenomena of graphite[16a,b] in the potential range of 0.2–0.02 V *vs.* Li|Li^+ as well (Figure S13b and S14b), which confirms the increased degree of graphitization. In particular, a sharpening of the de-/lithiation peaks with increasing activator content as well as with increasing temperature can be observed, which has also been discussed previously.[16a,b]

The Coulombic efficiency (C_{Eff}) of the initial charge/discharge cycles can be seen in Figure S15. In general, the initial C_{Eff} of all materials is relatively low (≈ 55–70%) and can lead to significant consumption of active lithium losses in a LIB full-cell setup. In previous works, the capacity loss in the first cycle was related to the electrolyte-accessible BET surface area of the electrode.[40] More recent works have also proven a stronger correlation for graphitic materials with the amount of edge/defect surface areas (non-basal) obtained by nitrogen adsorption measurements and adsorptive potential distributions according to DFT theory.[41] However, no clear trend was found here between C_{Eff} values and structural properties, *i.e.* BET surface area or 'non-basal plane' surface area. Nonetheless, values reported herein are consistent with values reported on previous works on catalytic graphitization using $FeCl_3$. Gomez-Martin *et al.* reported an initial C_{Eff} of only 64% when heat-treated the biomass precursor to 2000 °C.[16b] It is important to note that the acid washing step using HNO_3 to remove residual iron particles might also create some oxygen-surface groups that influence the initial C_{Eff}.[42] Further particle sizing and shaping, surface refinements or carbon coating approaches typically done in graphite anode material production could also
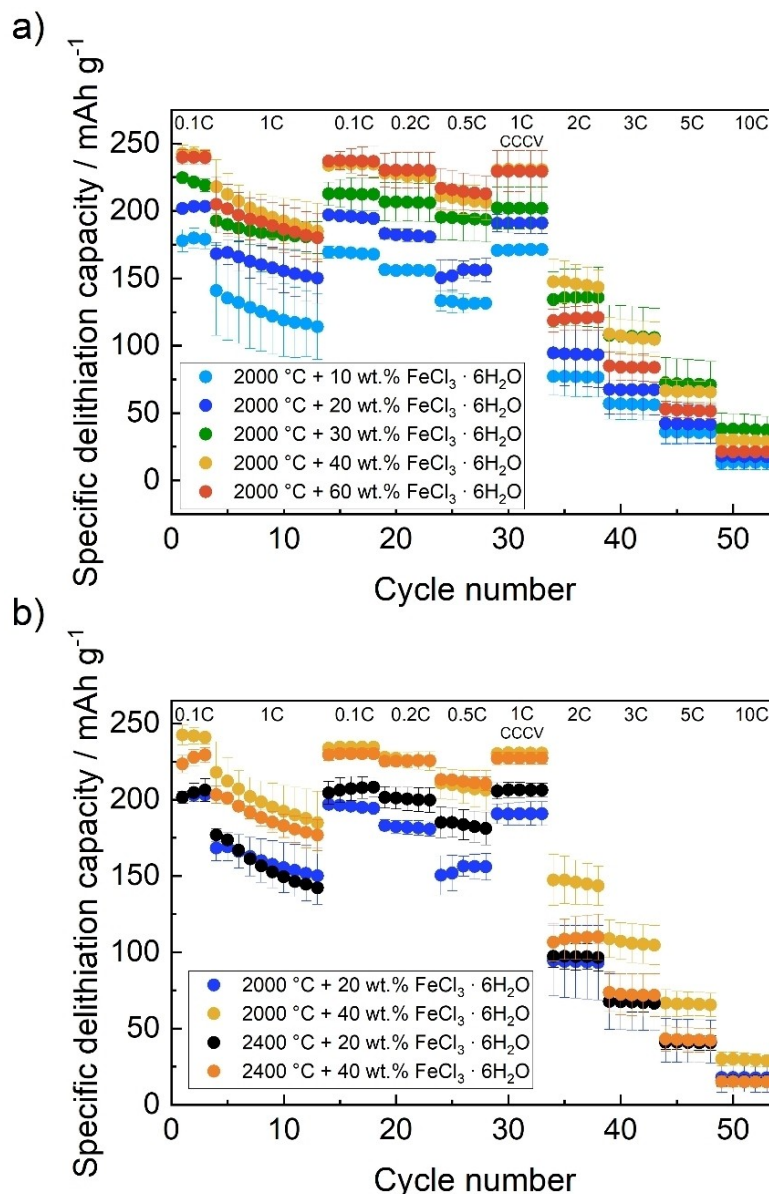
ChemElectroChem

Research Article
doi.org/10.1002/celc.202200819

**Chemistry
Europe**
European Chemical
Societies Publishing

Figure 7. Charge/discharge rate performance studies at rates between 0.1 and 10 C of carbon||Li metal cells for carbonaceous materials synthesized at 2000 °C and 2400 °C using 10 wt.% to 60 wt.% $FeCl_3 \cdot 6H_2O$ (three-electrode configuration, half-cell setup with Li metal as CE and RE). Electrolyte: 1 M $LiPF_6$ in EC/EMC (3:7) + 2 wt.% VC; potential range: 0.02 to 1.5 V vs. Li|Li^{+}. Cycles 28th–33rd performed using constant current/constant voltage conditions (CCCV) at 1 C. Error bars represent the standard deviation from three cells for each sample.

be addressed to achieve higher C_{Eff} values of biomass-derived synthetic graphite.[6a] However, these approaches would go far beyond the scope of this work and could only be performed in up-scaled material production processes (kg scale).

To get better insights into the impact of processing conditions on the electrochemical performance, Figure 8a, b shows the specific delithiation capacities of coffee ground-derived carbons at 0.1 C as a function of mass fraction of the activator iron chloride as well as degree of graphitization estimated from Raman fitting, respectively. Maximum reversible capacity values between 180 and 240 mAh g^{−1} are achieved. As can be seen, there is a gradual increase in achievable capacities when increasing the activator content up to 30 wt.% at 2000 °C

due to the increasing structural order within the carbon materials. In accordance with the changes of the structural properties, the specific delithiation capacity increases almost linearly with the iron chloride content, gaining ≈ 50 mAh g^{−1} per 10 wt.% $FeCl_3 \cdot 6H_2O$ as shown for the materials obtained at 2000 °C (Figure 8). Despite this, there appears to be a plateau in the specific capacity values and further increasing the initial iron chloride content above 40 wt.% or increasing the temperature above 2000 °C does not result in better electrochemical results. This trend is directly related to the estimated graphitization values from Raman measurements as can be seen in Figure 8b. Graphitization degrees of only 60–70% inevitably result in limited achievable specific capacities.
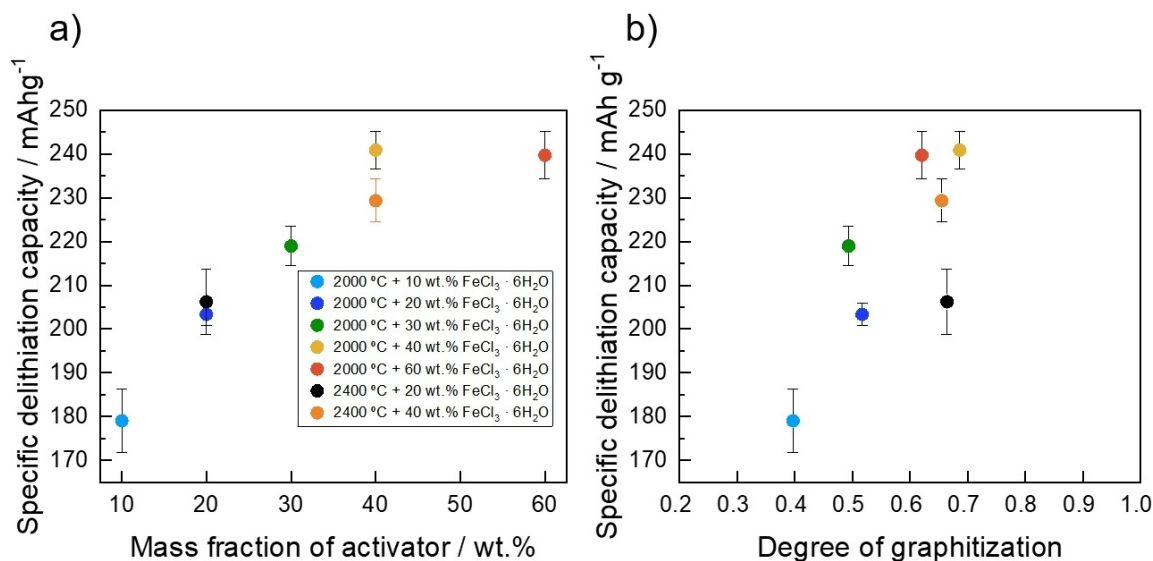
ChemElectroChem

Research Article
doi.org/10.1002/celc.202200819

**Chemistry
Europe**

European Chemical
Societies Publishing

Figure 8. Specific delithiation capacity at 0.1 C (2nd cyclee) of carbons in correlation to a) iron chloride content as well as b) degree of graphitization estimated from Raman fitting. Measured in a three-electrode cell configuration with Li metal as CE and RE, containing 1 M $LiPF_6$ in EC/EMC (3:7) + 2 wt.% VC in a potential range of 0.02 to 1.5 V *vs.* Li|Li$^+$.

Maximum reversible capacity values reported here are significantly lower than the theoretical capacity of graphite (372 mAh g^{-1}) or synthetic graphite synthetized using biomass and iron powder in recent studies.[23] Banek *et al.* recently reported the synthesis of highly crystalline flake graphite particles using hardwood sawdust and 62.5 wt.% iron powder by a laser pyrolysis.[23a] In that study, a maximum reversible capacity of 358 mAh g^{-1} was achieved in Li metal cells, which is similar than for commercial synthetic graphite materials. The limited degree of graphitization and achievable capacities reported here can be explained by the rapid volatility of iron chloride at higher temperatures, as there is almost no iron detected after graphitization at 2000 °C according to ICP-OES results (Table 1), or due to the biomass precursor itself. Other iron-based precursors with lower volatility tendency will be further investigated in future studies to reveal the impact on the degree of graphitization of biomass precursors and whether there is a limit for the graphitization of coffee ground.

Conclusions

Coffee ground-derived graphitic carbons were prepared by 'catalytic' graphitization in a temperature range of 1000 °C to 2400 °C introducing 10 to 60 wt.% of the activator iron (III) chloride hexahydrate ($FeCl_3 \cdot 6H_2O$) into the precursor material. A systematic investigation of the carbonaceous materials was conducted with special focus on the synthesis conditions, *i.e.*, heat treatment temperature and mass fraction of the activator, and their impact on the electrochemical performance in carbon||Li metal cells. The structural characterization showed that mass fractions of iron below 20 wt.% had only minor beneficial impact on the degree of graphitization, despite increasing heat treatment temperatures. In contrast, mass

fractions of $FeCl_3 \cdot 6H_2O$ equal to or above 20 wt.% facilitated the formation of a crystal structure just as an increased heat treatment temperature up to 2000 °C. However, temperatures above 2000 °C or initial concentration of iron chloride above 40 wt.% do not seem to have a significant impact on the formation of a more graphitic structure, indicating a saturation point in the graphitization of coffee ground. A maximum degree of graphitization of ≈ 69% was found for the carbon heat-treated at 2000 °C (40 wt.% activator). This study has reported for the first time a certain limit in terms of degree of graphitization using iron chloride as activator and coffee ground.

Electrochemical investigations were conducted for samples synthesized with 10 to 60 wt.% $FeCl_3 \cdot 6H_2O$ at 2000 °C as well as for samples obtained at 2400 °C (20 and 40 wt.% activator). The specific delithiation capacity of the carbons increases by 50 mAh g^{-1} per 10 wt.% $FeCl_3 \cdot 6H_2O$, while the electrochemical data of highly graphitized carbons feature both graphitic as well as amorphous characteristics in their potential profiles.

However, a maximum reversible capacity of ≈ 240 mAh g^{-1} was reported due to the limited degree of graphitization by 'catalytic' graphitization using iron chloride as activator. Higher values could not be reached either due to the 'non-graphitizable' nature of the coffee ground precursor material as a result of the initial strong cross-linking between carbon microcrystals or due to the iron chloride precursor itself. Future studies will investigate other types of activators (*e.g.*, iron nitrate, iron acetate and iron powder) as well as the impact of the particle size of the activator, which are going to have an impact on the decomposition temperature and homogeneity during heat treatment.

Experimental

The following carbonaceous materials were synthesized from coffee ground to investigate the impact of (i) the heat treatment temperature and (ii) the concentration of the activator ($FeCl_3 \cdot 6H_2O$) on the degree of graphitization and the electrochemical performance in carbon∣∣Li metal cells, as shown in Figure 9. Heat treatment temperatures between 1000 °C and 2400 °C and concentrations of activator between 0 and 60 wt.% were investigated.

Synthesis of carbonaceous materials

Coffee ground (*Caffè Crema Classico, Lavazza, Italy*) was used as organic waste precursor material for the preparation of carbonaceous materials. Therefore, dried precursor material was impregnated with a solution of $FeCl_3 \cdot 6H_2O$ (*Sigma Aldrich*; CAS-Nr.: 10025-77-1) in isopropanol (*Sigma Aldrich*; CAS-Nr.: 67-63-0) of the respective concentration. After evaporation of the solvent, the impregnated coffee ground was carbonized in an *RS 80/750/13 Nabertherm* oven (*Nabertherm GmbH*) under argon atmosphere with a gas flow of 100 $L h^{-1}$. All samples were heated up to 500 °C with a heating rate of 1 °C min^{-1}. The temperature was hold for 2 hours and further heated up to 1000 °C with a heating rate of 2 °C min^{-1}. The target temperature was hold for 10 hours to ensure total evaporation of small organic molecules. Subsequently, a second heat treatment was performed using a *LHTG 200-300/30-2G* oven (*Carbolite Gero GmbH & Co.KG*), whereby according to the applied temperature, the (partial) graphitization of the amorphous carbon occurs. Therefore, the respective heat treatment temperature (T_H) in the range of 1000 °C–2400 °C (Figure 9) was reached by a heating rate of 200 °C h^{-1} and hold for another 10 hours under argon atmosphere. Afterwards, the carbonaceous materials were stirred for 12 hours in concentrated HNO_3 (>69 %; *Sigma Aldrich*; CAS-Nr.: 7697-37-2) to remove the remaining activator. All samples were rinsed with deionized H_2O until a neutral pH-value was reached and dried in a *Binder* (*Binder GmbH*) oven at 80 °C. All powder samples were sieved to a grain size of 25 μm > x < 45 μm.

Characterization of carbonaceous materials

Thermogravimetric analyses were carried out to determine the initial mass loss of the coffee ground precursor during carbonization on a TGA Q5000 IR (*TA Instruments*). Analyses were conducted under argon atmosphere in a temperature range of 25 °C to 1200 °C with a heating rate of 2 °C min^{-1}.

Moreover, all samples were structurally characterized using Raman spectroscopy to determine the degree of graphitization with regard to the T_H and inserted mass fraction of $FeCl_3 \cdot 6H_2O$. Therefore, a Raman dispersive microscope (*Bruker SENTERRA, Bruker Optics Inc.*) with a green semiconductor laser, operating at a wavelength of 532 nm with a power of 10 mW, was used. A grating of 400 lines mm^{-1} was used as a dispersive element with a slit of 50 × 1000 μm as aperture. Both, the laser as well as the spectrometer were calibrated with a neon lamp. A CCD (charge-coupled device) detector with 1024 × 256 pixels, thermoelectrically cooled to −65 °C, was used. A microscope with a 20× objective was used to focus the samples. Each sample was measured at least five times, whereby for each spectrum ten integrations with an integration time of 60 seconds were performed. Raman spectra were deconvoluted using an in-house written code implemented in MATLAB and a non-linear least-squares fitting using pseudo-Voigt line-shape functions.

Furthermore, all samples were investigated by powder X-ray diffraction (PXRD) measurements using a *Bruker D8 Advanced X-ray powder diffractometer* (*Bruker AXS GmbH*) with a nickel filtered copper K_α-radiation with a wavelength of $\lambda = 0.154$ nm. Therefore, the respective sample was mixed with 10 wt.% of sieved pure Si powder (*Wacker Chemie*; grain size: 40–75 μm) as internal standard and spread onto an oriented Si-wafer sample holder. Thin layers of the samples were used to avoid any influence of adsorption. Measurements were performed in an angle range of 10 to 60° with a step width of $2\theta = 0.021°$. Instrumental contributions were corrected according to the procedure described by Iwashita et al.[33]

Scanning electron microscopy (SEM) analyses were carried out using a *Carl Zeiss AURIGA scanning electron microscope (Carl Zeiss*
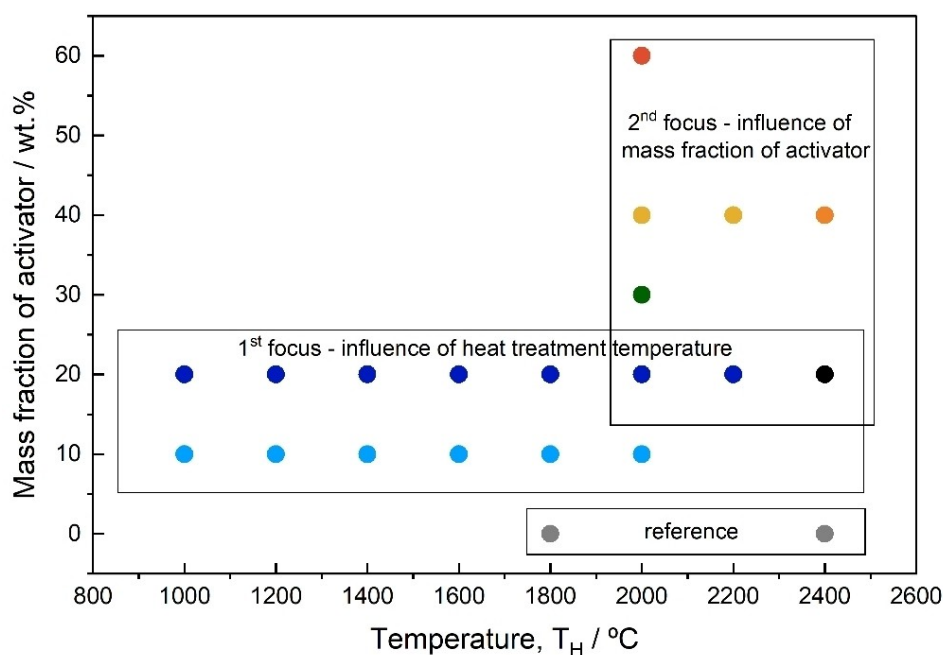

Figure 9. Overview of synthesized carbonaceous materials and considered focus in this work.

ChemElectroChem

Research Article
doi.org/10.1002/celc.202200819

Chemistry Europe
European Chemical
Societies Publishing

Microscopy GmbH) to evaluate the carbons' surface properties and particle morphologies.

Nitrogen adsorption measurements were carried out on a *3Flex* (*Micromeritics Instrument Corporation*) by use of liquid nitrogen at its boiling temperature of $-196\,°C$. All samples were degassed prior measurements at $250\,°C$ under reduced pressure (<0.05 mbar) for at least 12 h. The specific surface area and structural properties were calculated by the Brunauer-Emmett-Teller (BET) theory and density functional theory (DFT) based on the experimental data. The latter was especially applied for the determination of "basal", "prismatic" and "defect" surface areas in anisotropic graphitic structures by different adsorptive potentials.[35a,43]

ICP-OES measurements were conducted to determine the mass fraction of iron after carbonization and graphitization. Measurements were performed using an *ARCOS* (*Spectro Analytical Instruments GmbH*) with an axial positioned plasma torch. All other parameters were applied according to Vortmann and Evertz *et al.*[44]

Electrode preparation, cell assembly and electrochemical characterization

Composite electrodes consisting of 94 wt.% carbonaceous active material, 2 wt.% conductive agent Super C65 (*Imerys Graphite & Carbon*), 2 wt.% sodium-carboxymethyl cellulose (CMC) (*Walocel CRT 2000 PPA 12, Dow Wolff Cellulosics*) and 2 wt.% styrene-butadiene rubber (SBR) as binders (*LIPATON SB 5521, Synthomer*) on dendritic copper foil (*Carl Schlenk AG*) as current collector were prepared. First, SBR and CMC were stirred in deionized H_2O, followed by addition of Super C65 and the respective carbonaceous active material. After each additional component, the mixture was stirred for an hour to homogenize the electrode paste. A *Dispermat LC30 Motor type 5BCu2-042* (*VMA-Getzmann GmbH*) was applied with a speed of 10.000 rpm for an hour to avoid agglomeration of the particles. The resulting paste was coated onto dendritic cupper foil, using standard doctor-blade technique with a *ZUA 2000 Universal Applicator* (*ZEHNTER* GmbH) and an *Automatic Film Applicator 1133N* (*Sheen Instruments*) with a speed of $50\,mm\,s^{-1}$. The coated electrode sheets were dried at $80\,°C$ for 2 hours in a *Binder* (*Binder GmbH*) laboratory oven. Electrode discs with a diameter of 12 mm were punched from the dried sheets with a *Hohsen* electrode puncher (*Hohsen Corp.*). All electrodes were dried at $120\,°C$ for at least 12 hours under reduced pressure (<0.05 mbar) using a *Büchi Glass Oven B-585* (*Büchi Labortechnik*) to remove residual water. Afterwards, the electrodes were weighed using a *Sartorius ME 235S* analytical balance (*Sartorius AG*) with an accuracy of ±0.01 mg and stored at room temperature in a dry room (dew point of at least $-50\,°C$, 0.02% moisture content).

Electrochemical experiments of carbon||Li metal cells were performed in *Swagelok* T-cells with a three-electrode configuration (half-cell setup[38]), consisting of the respective working electrode (WE; $\varnothing=12$ mm) and Li metal (*Albemarle* Corporation) as counter (CE; $\varnothing=12$ mm) and reference electrodes (RE; $\varnothing=5$ mm). The cell body was electronically isolated by insulating *Mylar* foils. A *Freudenberg FS2190 polyolefin separator* was placed between WE and CE ($\varnothing=13$ mm, 6-layered, 120 μL electrolyte) as well as between RE and the main chamber of the three-electrode cell ($\varnothing=8$ mm, 3-layered, 80 μL electrolyte). 1 M $LiPF_6$ in a mixture of ethylene carbonate (EC) and ethyl methyl carbonate (EMC) in a ratio of 3:7 by weight (*BASF SE*; purity: battery grade) with 2 wt.% of the film forming additive vinylene carbonate (VC) was used as electrolyte. Electrochemical experiments were carried out using a *Maccor Series 4000 automated test system* (*Maccor Inc.*) at room temperature. The C-rate performances of the carbonaceous materials were investigated in carbon||Li metal cells by constant current charge/

discharge cycling (CCC) experiments applying different specific (dis)charge currents between 0.1 and 10 C within the potential range between 0.02 and 1.5 V *vs.* Li|Li$^+$. The specific current refers to the active mass loading of the respective electrode and the theoretical capacity of graphite ($372\,mAh\,g^{-1}$; $1\,C=372\,mA\,g^{-1}$), whereas the average active mass loading was $2.2\,mg\,cm^{-2}$ ($\pm$ $0.1\,mg\,cm^{-2}$). The cycling procedure was as follows: first, after initial resting for 6 hours, three formation cycles at 0.1 C were followed by 15 cycles at 1 C and five cycles at 0.1 C, 0.2 C and 0.5 C. Afterwards, five constant current constant voltage (CCCV) cycles at a potential of 20 mV *vs.* Li|Li$^+$ were performed at 1 C (current limitation: 0.5 C), followed by each five cycles at 2 C, 3 C, 5 C and 10 C. Three cells from each carbon sample were assembled and tested to ensure the reproducibility of the results. The standard deviation of each three cells is represented with the help of error bars in the corresponding figures.

Supporting Information

Supporting Information is available from the Wiley Online Library or from the author.

Conflict of Interest

The authors declare no conflict of interest.

Data Availability Statement

The data that support the findings of this study are available from the corresponding author upon reasonable request.

[1] a) S. Dühnen, J. Betz, M. Kolek, R. Schmuch, M. Winter, T. Placke, *Small Methods* **2020**, *4*, 2000039; b) M. Armand, P. Axmann, D. Bresser, M. Copley, K. Edström, C. Ekberg, D. Guyomard, B. Lestriez, P. Novák, M. Petranikova, W. Porcher, S. Trabesinger, M. Wohlfahrt-Mehrens, H. Zhang, *J. Power Sources* **2020**, *479*, 228708.
[2] a) P. Meister, H. Jia, J. Li, R. Klöpsch, M. Winter, T. Placke, *Chem. Mater.* **2016**, *28*, 7203; b) J. Asenbauer, T. Eisenmann, M. Kuenzel, A. Kazzazi, Z. Chen, D. Bresser, *Sustain. Energy Fuels* **2020**, *4*, 5387.

ChemElectroChem

Research Article
doi.org/10.1002/celc.202200819

Chemistry Europe
European Chemical
Societies Publishing

[3] T. Placke, G. G. Eshetu, M. Winter, E. Figgemeier, in *Lithium-ion Batteries Enabled by Silicon Anodes*, DOI: 10.1049/PBPO156E (Eds: C. Ban, K. Xu), The Institution of Engineering and Technology (IET) **2021**, p. 349.

[4] I. Cekic-Laskovic, N. von Aspern, L. Imholt, S. Kaymaksiz, K. Oldiges, B. R. Rad, M. Winter, *Top. Curr. Chem.* **2017**, *375*, 37.

[5] a) J. Kasnatscheew, R. Wagner, M. Winter, I. Cekic-Laskovic, *Top. Curr. Chem.* **2018**, *376*, 16; b) S. K. Heiskanen, J. Kim, B. L. Lucht, *Joule* **2019**, *3*, 2322.

[6] a) R. Schmuch, R. Wagner, G. Hörpel, T. Placke, M. Winter, *Nat. Energy* **2018**, *3*, 267; b) F. Duffner, N. Kronemeyer, J. Tübke, J. Leker, M. Winter, R. Schmuch, *Nat. Energy* **2021**, *6*, 123.

[7] J. Clark, *Webinar – 7th December 2020, Benchmark Mineral Intelligence* **2020**.

[8] a) *European Commission; https://ec.europa.eu/docsroom/documents/27348/attachments/1/translations/en/renditions/pdf* **2018**; b) P. Dolega, W. Bulach, J. Betz, S. Degreif, M. Buchert, *Policy Brief, Oeko-INstitut e.V.* **2021**.

[9] H. Jäger, W. Frohs, M. Banek, M. Christ, J. Daimer, F. Fendt, C. Friedrich, F. Gojny, F. Hiltmann, R. Meyer zu Reckendorf, J. Montminy, H. Ostermann, N. Müller, K. Wimmer, F. von Sturm, E. Wege, K. Roussel, W. Handl, in *Ullmann's Encyclopedia of Industrial Chemistry*, DOI: 10.1002/14356007.n05_n03, Wiley-VCH Verlag GmbH & Co. KGaA **2000**.

[10] *U. S. Department of the Interior, U. S. Geological Survey [https://www.usgs.gov/publications/mineral-commodity-summaries-2022]* **2022**.

[11] P. Dolega, M. Buchert, J. Betz, *Short study prepared within the framework of the BMBF joint project Fab4Lib, Oeko-Institut [https://www.oeko.de/en/publications/p-details/environmental-and-socio-economic-challenges-in-battery-supply-chains-graphite-and-lithium]* **2020**.

[12] A. D. McNaught, A. Wilkinson, *International Union of Pure and Applied Chemistry* **2014**, Version 2.3.3 [https://goldbook.iupac.org/].

[13] a) M. Wissler, *J. Power Sources* **2006**, *156*, 142; b) W. Lämmerer, H. Flachberger, *BHM Berg- und Hüttenmännische Monatshefte* **2017**, *162*, 336.

[14] S. M. Lee, D. S. Kang, J. S. Roh, *Carbon Lett.* **2015**, *16*, 135.

[15] G. Juri, H. A. Wilhelm, J. L'Heureux, *CFI Ceram. Forum Int.* **2007**, *84*, E22.

[16] a) O. Fromm, A. Heckmann, U. C. Rodehorst, J. Frerichs, D. Becker, M. Winter, T. Placke, *Carbon* **2018**, *128*, 147; b) A. Gómez-Martín, J. Martinez-Fernandez, M. Ruttert, A. Heckmann, M. Winter, T. Placke, J. Ramirez-Rico, *ChemSusChem* **2018**, *11*, 2776; c) L. Wu, D. Buchholz, C. Vaalma, A. G. Guinevere, S. Passerini, *ChemElectroChem* **2015**, *3*, 292; d) F. Luna-Lama, D. Rodríguez-Padrón, A. R. Puente-Santiago, M. J. Muñoz-Batista, A. Caballero, A. M. Balu, A. A. Romero, R. Luque, *J. Cleaner Prod.* **2018**, *207*, 411; e) H. Ru, N. Bai, K. Xiang, W. Zhou, H. Chen, X. S. Zhao, *Electrochim. Acta* **2016**, *194*, 10; f) W. X. Wang, Y. Wan, S. F. Wu, M. C. Li, L. J. Cao, F. C. Lv, M. Y. Yang, Z. F. Sun, R. Sun, Z. G. Lu, *RSC Adv.* **2015**, *5*, 46558.

[17] P. Ouzilleau, A. E. Gheribi, P. Chartrand, G. Soucy, M. Monthioux, *Carbon* **2019**, *149*, 419.

[18] a) Q. Yan, J. Li, X. Zhang, E. B. Hassan, C. Wang, J. Zhang, Z. Cai, *J. Nanopart. Res.* **2018**, *20*, 223; b) A. Gómez-Martín, J. Martinez-Fernandez, M. Ruttert, M. Winter, T. Placke, J. Ramirez-Rico, *ACS Omega* **2019**, *4*, 21446; c) A. Oya, H. Marsh, *J. Mater. Sci.* **1982**, *17*, 309; d) Y. C. Liu, Q. L. Liu, J. J. Gu, D. M. Kang, F. Y. Zhou, W. Zhang, Y. Wu, D. Zhang, *Carbon* **2013**, *64*, 132; e) A. Gomez-Martin, Z. Schnepp, J. Ramirez-Rico, *Chem. Mater.* **2021**, *33*, 3087; f) R. Hunter, J. Rowlandson, G. J. Smales, B. R. Pauw, V. Ting, A. N. Kulak, Z. Schnepp, *Mater Adv* **2020**, *1*, 3281.

[19] K. J. Laidler, *Pure Appl. Chem.* **1996**, *68*, 149.

[20] a) F. J. Maldonado-Hódar, C. Moreno-Castilla, J. Rivera-Utrilla, Y. Hanzawa, Y. Yamada, *Langmuir* **2000**, *16*, 4367; b) C. J. Thambiliyagodage, S. Ulrich, P. T. Araujo, M. G. Bakker, *Carbon* **2018**, *134*, 452.

[21] a) R. Othman, A. S. Kamal, N. H. Jabarullah, *Prod. Eng. Arch.* **2021**, *27*, 124; b) A. Gutiérrez-Pardo, J. Ramírez-Rico, R. Cabezas-Rodríguez, J. Martínez-Fernández, *J. Power Sources* **2015**, *278*, 18; c) J. Hoekstra, A. M.

Beale, F. Soulimani, M. Versluijs-Helder, J. W. Geus, L. W. Jenneskens, *J. Phys. Chem. C* **2015**, *119*, 10653; d) J. Hoekstra, A. M. Beale, F. Soulimani, M. Versluijs-Helder, D. van de Kleut, J. M. Koelewijn, J. W. Geus, L. W. Jenneskens, *Carbon* **2016**, *107*, 248.

[22] W. J. Sagues, J. Yang, N. Monroe, S.-D. Han, T. Vinzant, M. Yung, H. Jameel, M. Nimlos, S. Park, *Green Chem.* **2020**, *22*, 7093.

[23] a) N. A. Banek, K. R. McKenzie, D. T. Abele, M. J. Wagner, *Sci. Rep.* **2022**, *12*, 8080; b) N. A. Banek, D. T. Abele, K. R. McKenzie, M. J. Wagner, *ACS Sustainable Chem. Eng.* **2018**, *6*, 13199.

[24] S. I. Mussatto, E. M. S. Machado, S. Martins, J. A. Teixeira, *Food Bioproc. Tech.* **2011**, *4*, 661.

[25] S. B. Kanungo, S. K. Mishra, *J. Therm. Anal.* **1996**, *46*, 1487.

[26] A. C. Ferrari, J. Robertson, *Phys. Rev. B* **2000**, *61*, 14095.

[27] F. Tuinstra, J. L. Koenig, *J. Chem. Phys.* **1970**, *53*, 1126.

[28] a) A. Sadezky, H. Muckenhuber, H. Grothe, R. Niessner, U. Pöschl, *Carbon* **2005**, *43*, 1731; b) G. Katagiri, H. Ishida, A. Ishitani, *Carbon* **1988**, *26*, 565.

[29] M. A. Pimenta, G. Dresselhaus, M. S. Dresselhaus, L. G. Cançado, A. Jorio, R. Saito, *Phys. Chem. Chem. Phys.* **2007**, *9*, 1276.

[30] L. G. Cançado, K. Takai, T. Enoki, M. Endo, Y. A. Kim, H. Mizusaki, A. Jorio, L. N. Coelho, R. Magalhães-Paniago, M. A. Pimenta, *Appl. Phys. Lett.* **2006**, *88*, 163106.

[31] J. Ramirez-Rico, A. Gutierrez-Pardo, J. Martinez-Fernandez, V. V. Popov, T. S. Orlova, *Mater. Des.* **2016**, *99*, 528.

[32] A. Gomez-Martin, J. Martinez-Fernandez, M. Ruttert, M. Winter, T. Placke, J. Ramirez-Rico, *Chem. Mater.* **2019**, *31*, 7288.

[33] N. Iwashita, C. R. Park, H. Fujimoto, M. Shiraishi, M. Inagaki, *Carbon* **2004**, *42*, 701.

[34] Y. Waseda, E. Matsubara, K. Shinoda, in *X-Ray Diffraction Crystallography: Introduction, Examples and Solved Problems*, DOI: 10.1007/978-3-642-16635-8_3 (Eds: Y. Waseda, E. Matsubara, K. Shinoda), Springer Berlin Heidelberg, Berlin, Heidelberg **2011**, p. 67.

[35] a) T. Placke, V. Siozios, R. Schmitz, S. F. Lux, P. Bieker, C. Colle, H. W. Meyer, S. Passerini, M. Winter, *J. Power Sources* **2012**, *200*, 83; b) T. Placke, V. Siozios, S. Rothermel, P. Meister, C. Colle, M. Winter, *Z. Phys. Chem.* **2015**, *229*, 1451.

[36] K. S. W. Sing, *Pure Appl. Chem.* **1985**, *57*, 603.

[37] S. Glatzel, Z. Schnepp, C. Giordano, *Angew. Chem. Int. Ed.* **2013**, *52*, 2355.

[38] R. Nölle, K. Beltrop, F. Holtstiege, J. Kasnatscheew, T. Placke, M. Winter, *Mater. Today* **2020**, *32*, 131.

[39] a) S. R. Sivakkumar, J. Y. Nerkar, A. G. Pandolfo, *Electrochim. Acta* **2010**, *55*, 3330; b) M. Winter, J. O. Besenhard, *Handbook of Battery Materials (Eds.: Daniel, C.; Besenhard, J. O.)* **2011**, Second Edition, 433.

[40] S. H. Ng, C. Vix-Guterl, P. Bernardo, N. Tran, J. Ufheil, H. Buqa, J. Dentzer, R. Gadiou, M. E. Spahr, D. Goers, P. Novák, *Carbon* **2009**, *47*, 705.

[41] a) K. Persson, V. A. Sethuraman, L. J. Hardwick, Y. Hinuma, Y. S. Meng, A. van der Ven, V. Srinivasan, R. Kostecki, G. Ceder, *J. Phys. Chem. Lett.* **2010**, *1*, 1176; b) T. Placke, V. Siozios, R. Schmitz, S. F. Lux, P. Bieker, C. Colle, H. W. Meyer, S. Passerini, M. Winter, *J. Power Sources* **2012**, *200*, 83; c) T. Placke, V. Siozios, S. Rothermel, P. Meister, C. Colle, M. Winter, *Z. Phys. Chem.* **2015**, *229*, 1451.

[42] A. Gomez-Martin, A. Gutierrez-Pardo, J. Martinez-Fernandez, J. Ramirez-Rico, *Fuel Process. Technol.* **2020**, *199*, 106279.

[43] J. P. Olivier, M. Winter, *J. Power Sources* **2001**, *97–8*, 151.

[44] a) M. Evertz, J. Kasnatscheew, M. Winter, S. Nowak, *Anal. Bioanal. Chem.* **2019**, *411*, 277; b) B. Vortmann-Westhoven, M. Winter, S. Nowak, *J. Power Sources* **2017**, *346*, 63.